Heliyon 10 (2024) e24070

Contents lists available at ScienceDirect

Heliyon

journal homepage: www.cell.com/heliyon

Research article

Cobalt-nickel phosphide supported on reduced graphene oxide for sensitive electrochemical detection of bisphenol A

Isilda Amorim [a,b,*], Zhipeng Yu [b], Lifeng Liu [b], Fátima Bento [a]

[a] Centre of Chemistry, University of Minho, Gualtar Campus, Braga, 4710-057, Portugal
[b] Clean Energy Cluster, International Iberian Nanotechnology Laboratory (INL), Avenida Mestre Jose Veiga, 4715-330, Braga, Portugal

ARTICLE INFO

Keywords:
Transition metal phosphide
Reduced graphene oxide
Electrochemical sensor
Water pollution
Hydroquinone
Bisphenol A

ABSTRACT

Bisphenol A (BPA) is a commonly utilized phenolic contaminant in several manufacturing processes, contributing to environmental pollution. Therefore, the detection of BPA holds significant importance for monitoring water quality. In this work, we report a robust electrochemical detection method for BPA utilizing cobalt–nickel bimetal phosphide nanoparticles (CoNiP) supported on reduced graphene oxide (rGO). The CoNiP@rGO-modified glassy carbon electrode exhibits remarkable electrochemical activity in BPA detection. The detection mechanism is controlled by adsorption-mediated electron transfer, showcasing a low limit of detection (LOD) at 0.38 nM and a high sensitivity of 96.4 A M^{-1} cm^{-2} within the linear range of 0.001–8 μM. Furthermore, our developed sensor demonstrates good reproducibility and successfully detected BPA in actual water samples. The electrochemical activity of CoNiP@rGO was also characterized for hydroquinone (HQ) detected through a diffusion-controlled mechanism, displaying an excellent sensitivity of 36.4 A M^{-1} cm^{-2} across a broad linear range. These findings underscore the promising potential of CoNiP@rGO as a candidate for electrochemical detection of phenolic contaminants, especially in the sensing of BPA in environmental water samples. This efficacy is attributed to the modulation of its electronic properties, combined with its large electroactive surface area and low electron-transfer resistance.

1. Introduction

The escalating challenges posed by rapid population growth and industrialization have significantly contributed to environmental pollution, jeopardizing ecosystems and inflicting toxic effects on various organisms, including humans. Phenolic compounds, extensively utilized in diverse industries, are of particular concern due to their enduring presence in the environment, owing to their non-degradable nature [1]. Moreover, their water solubility raises the risk of contaminating potable water sources [2]. Bisphenol A (BPA), among numerous phenolic compounds, has earned priority pollutant status from both the US Environmental Protection Agency (US EPA) and the European Commission (EC) due to its inherent toxicity [3]. BPA is prevalent in the manufacturing of various products (such as polycarbonate plastics, food packaging materials, epoxy resins, medical devices, thermal papers and dental sealants) [4] and can leach into the environment, potentially rising human exposure through dietary or water intake [4]. Functioning as an endocrine-disrupting chemical, even at minimal concentrations, it can mimic or block the endogenous hormones, contributing to

* Corresponding author. Centre of Chemistry, University of Minho, Gualtar Campus, Braga, 4710-057, Portugal. Clean Energy Cluster, International Iberian Nanotechnology Laboratory (INL), Avenida Mestre Jose Veiga, 4715-330, Braga, Portugal
E-mail address: isilda.amorim@inl.int (I. Amorim).

https://doi.org/10.1016/j.heliyon.2024.e24070
Received 19 October 2023; Received in revised form 15 December 2023; Accepted 3 January 2024
Available online 7 January 2024

diverse health issues, including cancer, depression, obesity, and infertility [4,5]. Acknowledging the high risk and potential exposure to BPA, the European Parliament and the Council, through directive (EU) 2020/2184, stipulated that BPA must not exceed a parametric value of 2.5 μg L^{-1} (0.01 μM) in water intended for human consumption. Hence, achieving high-sensitivity at low concentrations is paramount.

Electrochemical sensing emerges as a cost-effective, highly selective, easily operable, and efficient solution, offering swift response times for target analyte detection. Various electrode materials have been explored for BPA detection, including transition metal oxides [6–8], sulfides [9,10] selenides [11,12], carbon materials [13–15], and noble metals [16–18], aiming to enhance the performance of electrocatalytic and analytical sensors. However, the existing sensors fall short of meeting the mandated parametric value. Consequently, there is a compelling need to explore new electrode materials for BPA electrochemical sensing with detection limits (LOD) and quantification limits (LOQ) aligned with the established parametric value.

Transition metal phosphides (TMPs) emerged as promising electrode materials, detecting various molecules thanks to their metalloid properties, structural stability, natural abundance, and cost-effectiveness [19]. For instance, copper phosphide nanowire on copper foam (Cu_3P NW/CF) demonstrated enzymless glucose detection with a LOD of 0.32 μM [20]. Similarly, Ni_2P nanosheets array on Ti mesh (Ni_2P NA/TM) showcased H_2O_2 sensing with a sensitivity of 0.6907 A M^{-1} cm^{-2} [21]. TMPs have also proven to be effective in detecting phenolic molecules withor great sensitivity, selectivity and low LOD, such as N and FeP co-doped carbon nanotube (N/FeP-CNT) for dihydroxybenzoic acid isomers [22] and N,P co-doped glucose-derived carbon coated CoP nanowires (G-CoP/N,P–C NWs) to simultaneously determine hydroquinone and catechol [23]. Similarly, MOF-derived nanoparticles embedded in N-doped porous carbon (CoP_x@NCNTs) [24] and Co_xP nanoparticles embedded in three-dimensional carbon microspheres (Co_xP/NC) [25] have been employed for 4-nitrophenol detection.

Graphene with its highly ordered structure, remarkable surface areas (up to 2630 m^2 g^{-1}), and exceptional thermal conductivity (5000 W mK^{-1}), stands out as a leading candidate for the advancement of cutting-edge carbon-based materials [26]. However, the cost-effective and large-scale production of premium-grade graphene persists as a noteworthy challenge. To address this, graphene oxide (GO), a derivative of graphene, offers a more cost-efficient and rapid solution on an industrial scale. GO sharing a 2D structure with graphene, features carbon atoms functionalized with groups containing oxygen functionalities (e.g. hydroxyl, carbonyl) on the edges and basal plane [27]. Although GO exhibits lower conductivity than graphene, its properties can be substantially enhanced through reduction processes, leading to the formation of reduced graphene oxide (rGO) [28]. This creates a promising compromise, offering improved conductivity while retaining many advantageous properties of graphene. In comparison to other 2D materials like graphitic carbon nitride (g-C_3N_4), MXenes, and layered double hydroxides (LDHs), rGO holds several advantages. These alternative materials face challenges such as poor conductivity and dispersibility [29], low stability in colloidal solutions and stiffness [30,31], and low electronic conductivity and slow electron transfer rates [31], respectively.

Furthermore, the presence of oxygen moieties on rGO and structural defects allows for surface functionalization with transition metals enhancing sensor performance [32,33]. In this sense, carbon-based materials, including carbon nanotubes (CNTs), GO and rGO, have been utilized to anchor TMPs. This approach improves stability by preventing dissolution and/or agglomeration of materials deposited at the electrode surface [34–36]. Additionally, the electrical conductivity can be enhanced, and the electronic state of TMPs modulated in the presence of carbonaceous supports. The strong metal-carbon support interactions contribute to improved electron transfer kinetics at the metal/graphene interface [37].

To the best of our knowledge, the utilization of TMPs for BPA detection has not been reported, despite their demonstrated enhanced sensitivity in detecting several biologically and environmentally relevant molecules, including phenolic compounds. The detection of BPA poses a significant challenge due to the stringent lower limits set by the European Parliament and the Council. Indeed, there is a

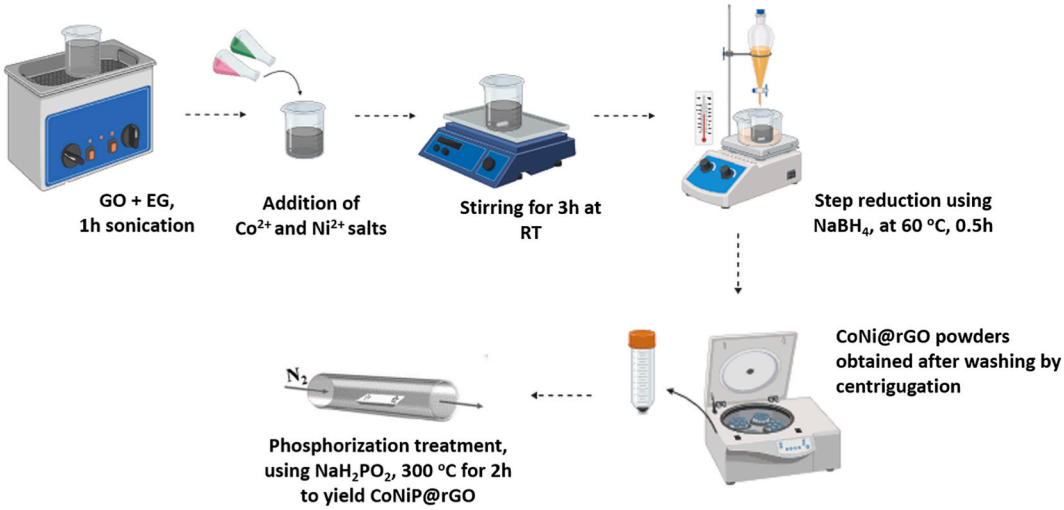

Scheme 1. Schematic illustration for the synthesis of CoNiP@rGO.

scarcity of sensor devices with adequate detection thresholds low enough to meet the settled parametric values [6,38–41].

In previous work in the laboratory, we optimized a composite based on nanoparticles of cobalt and nickel phosphide anchored on rGO (CoNiP@rGO), demonstrating superior electrocatalytic performance for electrochemical sensing compared to other prepared materials (e.g. CoNiP; rGO; CoNi and CoNi@rGO) [42]. Building upon these findings, the present work reports CoNiP@rGO-modified glassy carbon electrodes, incorporating an enhanced measurement methodology involving analyte adsorption prior to electron transfer. This methodology proves the ability to detect BPA at concentrations below the established parametric values. The sensing capabilities of CoNiP@rGO are also illustrated for hydroquinone, a non-adsorbing polyphenol, which demonstrated excellent electrocatalytic activity with low LOD and high sensitivity. Moreover, the designed electrochemical sensor successfully detects BPA in real samples, including tap water and plastic bottled mineral water.

2. Experimental section

2.1. Synthesis of cobalt–nickel phosphide on rGO

All chemicals employed in this study were of analytical grade and utilized in their original state. The synthesis of material involved a chemical reduction, in ethylene glycol (EG) solution, of the respective metal cations using sodium borohydride ($NaBH_4$), as illustrated in Scheme 1 [43]. Specifically, 25 mL of 4 mg mL^{-1} solution of commercial graphene oxide (GO) in H_2O (Sigma-Aldrich) was initially mixed with 12.5 mL of EG and subjected to sonication for 1 h at 25 °C. After the addition of EG solutions containing 0.05 M $Co(NO_3)_2{\cdot}6H_2O$ (4.3 mL) and 0.05 M $Ni(NO_3)_2{\cdot}6H_2O$ (4.3 mL) to the GO solution, the resultant mixture was stirred for 3 h at room temperature. The temperature of the solution was then raised to 60 °C in an oil bath and 12.5 mL of $NaBH_4$ solution (30 mg mL^{-1}) was added dropwise under vigorous stirring. After reacting for 0.5 h, the mixture was cooled to 25 °C, subjected to centrifugation and washed repeatedly with ultrapure water with a resistivity of 18.2 MΩ cm, to obtain CoNi@rGO powders. The resulting powders were subsequently dried at 80 °C using a vacuum oven. The phosphorization process was carried out using NaH_2PO_2 as the phosphorus source. Usually, CoNi@rGO (0.1 g) was placed in a ceramic boat and positioned 2 cm away from NaH_2PO_2 (0.5 g) which was on the upstream side. The boat was then inserted into a tubular furnace, where N_2 with high-purity (99.999 %) flowed at a rate of 800 SCCM for 1 h to remove oxygen. Subsequently, the temperature of the furnace was slowly increased to 300 °C (rate of 5 °C min^{-1}), maintained at this temperature for 2 h, and then naturally cooled to ambient temperature. A continuous flow of N_2 was held throughout the entire reaction.

2.2. Electrode preparation and electrochemical measurements

The catalyst ink was prepared by dispersing 5 mg of CoNiP@rGO in 1 mL of ultrapure water using an Hielscher UP50H ultrasonic probe (50 W at 60 % of amplitude). In the sensor preparation, 5 μL of the CoNiP@rGO ink was drop-cast onto a glassy carbon electrode (GCE) (3 mm in diameter) with a polished surface, resulting in a mass loading density of approximately 0.3 mg cm^{-2}. Subsequently, the modified electrode surface was exposed to an incandescent lamp to evaporate the solvent. A three-electrode setup (at room temperature) was used in the electrochemical assays on a PGSTAT 30 Autolab from Ecochemie (The Netherlands) interfaced with a computer operating with a "General Purpose Electrochemical System'' software (version 4.9). The working electrode was the GCE loaded with CoNiP@rGO, with a Pt wire serving as the counter electrode and an Ag/AgCl electrode (KCl saturated) as the reference electrode. The supporting electrolyte used was a solution of 0.1 M of phosphate buffer (PBS) at pH = 7.0.

The electrochemical behaviour of both the GCE and CoNiP@rGO were characterized by cyclic voltammetry (CV) in the potential window of −0.1 to 0.5 V *vs* Ag/AgCl, *sat.* using scan rates from 20 to 400 mV s^{-1} in a 0.1 M KCl solution containing 3.0 mM $K_3[Fe(CN)_6]$.

For BPA detection, CV measurements were performed in 250 or 500 μM of BPA solution containing 0.1 M PBS, at a scan rate (υ) of 20 mV s^{-1}. Differential pulse voltammetry (DPV) was conducted from 0.1 to 0.7 V with a modulation amplitude of 100 mV and a step potential of 10 mV, with an interval time of 0.5 s and modulation time of 0.05 s, including an accumulation step at 0 V for 500 s before DPV measurements.

For hydroquinone (HQ) detection, CV measurements were carried out using 500 μM HQ solution in 0.1 M PBS, at a scan rate (υ) of 20 mV s^{-1}. DPV was performed from −0.2 to 0.3 V with a modulation amplitude of 25 mV and a step potential of 5 mV, with an interval time of 0.5 s and modulation time of 0.05 s. Electrochemical impedance spectroscopy (EIS) was acquired at room temperature with a Biologic VMP-3 potentiostat/galvanostat, with a frequency range from 10 mHz to 100 kHz and a signal amplitude of 10 mV, all in a 500 μM HQ solution.

For the electrochemical measurements, solutions of HQ and BPA were prepared by diluting 0.1 M BPA (in ethanol) or 0.1 M HQ (aqueous) stock solutions, both stored at −22 °C, with 0.1 M PBS (pH 7.0).

2.3. Samples preparation

Laboratory-collected tap water samples and mineral bottled water samples obtained from a local supermarket, were utilized without any pre-treatment. For the direct determination of BPA, 9 mL of water sample was directly diluted in 1 mL of 1 M PBS solution. Then, these solutions were spiked with known quantities of BPA (2 and 4 μM), and then analysed by DPV to determine the recovery rate. Each sample underwent three independent experiments for robust analysis.

3. Results and discussion

3.1. Characterization of CoNiP@rGO

The morphology, microstructure and chemical surface of CoNiP@rGO have been previously elucidated by our group [42]. In brief, transmission electron microscopy (TEM) characterization of CoNiP nanoparticles densely dispersed on rGO revealed an average size of 6.4 nm. Distinct lattice fringes corresponding to the crystal planes of hexagonal CoNiP (ICDD no. 04-001-6153) were observed, emphasizing the well-defined structure. Elemental mapping confirmed the presence of Co, Ni and P elements evenly covering the rGO surface. X-ray diffraction (XRD) further affirmed that a CoNiP solid solution was obtained, with diffraction peaks aligning with hexagonal CoNiP (ICDD No. 04-001-6153). X-ray photoelectron spectroscopy provided additional evidence of phosphides formation, revealing binding energy peaks related to metal phosphides in the Co 2p, Ni 2p and P 2p spectra. The C 1s spectrum of CoNiP@rGO showcased a pronounced peak at 284.6 eV, indicating a high degree of graphitization with sp^2-hybridized graphitic carbon (C–C bond). The positive shift in binding energies of Co 2p, Ni 2p and P 2p in CoNiP@rGO compared to unsupported CoNiP suggested a synergistic interaction between the rGO and the metal phosphide.

The electrochemical behaviour of CoNiP@rGO as an electrode material was elucidated through cyclic voltammetry (CV) using the Fe(III)/Fe(II) system in 0.1 M KCl electrolyte. The obtained electrochemical response, from both bare GCE and CoNiP@rGO is characteristic of a one-electron reversible process (Fig. 1a), exhibited a unitary ratio of cathodic to anodic peak currents, $I_{pc}/I_{pa} = 1.0$, and a peak-to-peak separation (ΔE_p) close to 60 mV (Fig. 1a). Additionally, the electroactive surface area (ESA), calculated from the representation of peak current against the square root of the scan rate ($\upsilon^{1/2}$) (Fig. 1b), increased from 4.4 mm^2 to 6.2 mm^2 upon GCE modification with CoNiP@rGO. The ESA was determined using the Randles-Sevcik equation ($I_p = 2.69 \times 10^5 \times n^{3/2} A D^{1/2} \upsilon^{1/2} C$),

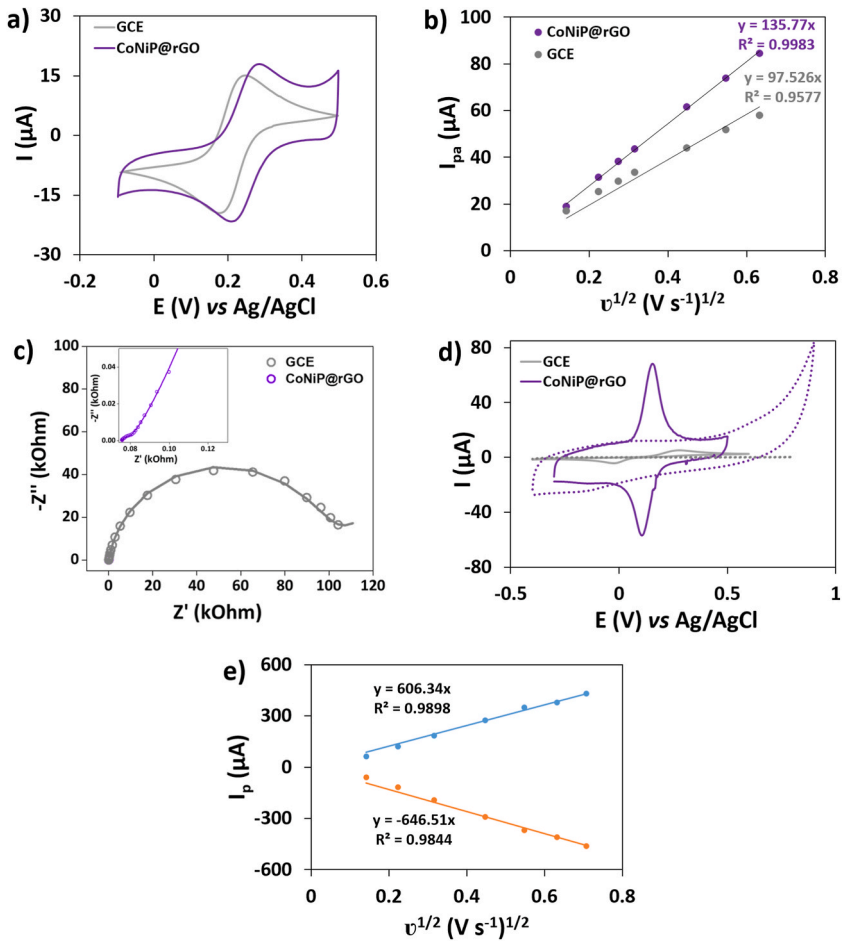

Fig. 1. (a) Cyclic voltammograms of bare GCE and CoNiP@rGO/GCE recorded at 20 mV s^{-1} in 3.0 mM $K_3[Fe(CN)_6]$ with 0.1 M KCl. (b) I_{pa} *vs* $\upsilon^{1/2}$ from a 3.0 mM $K_3[Fe(CN)_6]$ solution. (c) Nyquist plots obtained in 0.1 M PBS containing 500 μM HQ. The inset represents the Nyquist plot of CoNiP@rGO/GCE. Scattered points correspond to experimental data and solid lines represent fitting curves. (d) Voltammetric response of bare GCE and CoNiP@rGO/GCE recorded at 20 mV s^{-1} in 0.1 M PBS (dotted lines) and in the presence of 500 μM HQ (full lines). (e) I_p *vs* $\upsilon^{1/2}$ from CoNiP@rGO/GCE in 500 μM HQ solution.

where n represents the number of electrons ($n = 1$ for a one-electron transfer reaction), A denoted the electroactive surface area (in cm^2), D is the diffusion coefficient ($D = 7.6 \times 10^{-6}$ cm^2 s^{-1} in 0.1 M KCl) [44], C stands to the bulk concentration of $K_3[Fe(CN)_6]$ (in mol cm^{-3}), and υ is the scan rate (in V s^{-1}).

The impact of the electrode modification on charge transfer kinetics was assessed through electrochemical impedance spectroscopy (EIS) of CoNiP@rGO and GCE, as depicted in Fig. 1c. The smaller semicircle domains observed for CoNiP@rGO signify a lower charge-transfer resistance. Fitting the data with a Randles equivalent circuit yielded a minimal resistance value of only 4.2 Ohm, underscoring the enhanced charge transfer facilitated by CoNiP@rGO.

The analytical performance of the CoNiP@rGO/GCE sensor was evaluated using hydroquinone (HQ) as a model polyphenol molecule. Beyond its role as a model, the HQ detection holds environmental significance as it is a prevalent pollutant found in dyes, cosmetics, antioxidants, and secondary colouring agents [45].

Fig. 1d displays the CV voltammograms of GCE and CoNiP@rGO/GCE in the presence and absence of HQ in 0.1 M PBS. In the presence of HQ, distinct redox peaks associated with electrochemical reactions of HQ are evident in the CVs of both bare GCE and CoNiP@rGO/GCE. Surface modification significantly impacted both residual and faradaic currents. The residual current, represented as dotted lines, witnessed a substantial increase due to the augmented charge storage capacity at the interface, a consequence of the microstructure of the CoNiP@rGO/GCE sensor. Concurrently, electrode modification led to a noteworthy rise of the redox peak currents and a diminution in peaks separation, associated with the electrocatalytic activity of CoNiP@rGO in the oxidation of HQ. This enhancement resulted in more favourable electron transfer kinetics and a diminished charge-transfer resistance. The influence of scan rate on the HQ redox peak current was further investigated for CoNiP@rGO/GCE, ranging from 20 to 400 mV s^{-1} (Fig. 1e). The peak current intensity (I_p) increase linearly with the square root of scan rate ($\upsilon^{1/2}$) which indicates that the HQ electrochemical reactions are controlled by diffusion, further emphasizing the sensor's robust electrochemical performance.

The analytical performance of the CoNiP@rGO/GCE sensor for the quantification of HQ was investigated through DPV. The recorded voltammograms for diverse standard concentrations of HQ are presented in Fig. 2a. The outcomes illustrate a linear increase in peak current with concentration (Fig. 2b), showcasing a substantial sensitivity of 36.4 A M^{-1} cm^{-2} in HQ detection. The limits of detection (LOD) and quantification (LOQ) were calculated using **equations 1** and **2**, respectively:

$$\mathrm{LOD} = \frac{3\sigma}{m} \tag{1}$$

$$\mathrm{LOQ} = \frac{10\sigma}{m} \tag{2}$$

where σ is the standard deviation of I_p from the standard solution with the lowest HQ concentration (n = 4) and m represents the slope of the calibration plot. Calculated values for LOD and LOQ are 0.5 μM and 1.77 μM, respectively.

The sensitivity of determination is remarkably high and the analytical thresholds are considerably lower compared to electrodes modified with other materials reported in literature, such as copper oxide and carbon nano-fragment modified glassy carbon electrode (CuO–CNF/GCE) [46], Au@Pd core-shell nanocomposites [47] and carbon nanocages (CNCs)-reduced graphene oxide (RGO) [48]. For

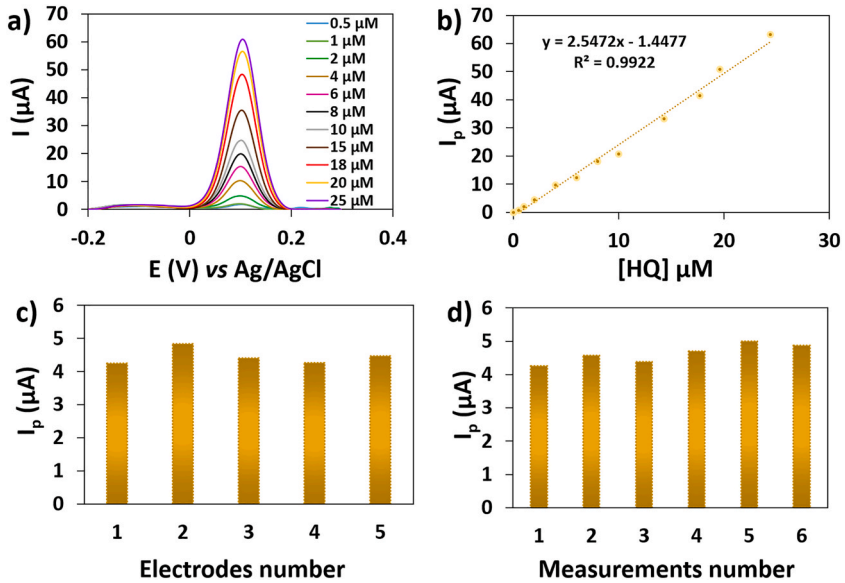

Fig. 2. DPV results of CoNiP@rGO/GCE in 0.1 PBS solutions containing HQ: (a) Voltammograms obtained for standard solutions of different concentrations; (b) Peak currents as a function of HQ concentration; Peak currents registered from a 2 μM HQ solution for (c) five independent electrodes and for (d) six consecutive measurements at a single electrode.

these materials, sensitivities and LOD were reported as follows: 0.382 A M^{-1} and 1 μM; 1.496 A M^{-1} and 0.63 μM; 0.0726 A M^{-1} and 0.87 μM, respectively.

Precision estimates for CoNiP@rGO/GCE were determined from reproducibility and repeatability data. A reproducibility of 4.8 % was obtained from the relative standard deviation (RSD) of five independently prepared CoNiP@rGO/GCE sensors (Fig. 2c). Repeatability, calculated as the RSD of six consecutive measurements using the same electrode, was 5.6 % (Fig. 2d). These precision results are comparable to, or even lower than those reported in the literature for other electrode materials, confirming the reliability of CoNiP@rGO for the quantification of HQ [49–51].

3.2. Electrochemical behaviour of CoNiP@rGO for BPA detection

The electrochemical response to BPA was inspected through cyclic voltammetry (CV) for both bare glassy carbon electrode (GCE) and GCE modified with CoNiP@rGO (CoNiP@rGO/GCE) in 0.1 M PBS solution containing 500 μM and 250 μM of BPA, respectively. Background currents of the bare GCE and CoNiP@rGO/GCE are displayed in Fig. 3a, revealing the absence of faradaic process, except for the small peaks at around 0.35 V, characteristic of graphene oxidation/reduction [52,53]. The voltammetric curves for BPA oxidation at both electrodes exhibit a single peak in the anodic scan (Fig. 3b), indicating the irreversibility of BPA oxidation. In addition to the BPA oxidation peak, the CoNiP@rGO/GCE voltammogram displays two additional small peaks associated with graphene oxidation/reduction, akin to those observed in the blank solution. The anodic peak current (with an equivalent sensitivity of I_{pa}/C of 3.6 mA M^{-1}) at a high positive oxidation potential (E_{pa}) around 0.55 V against Ag/AgCl, *sat.* recorded on the GCE suggests its unsuitability for the sensitive detection of BPA. In contrast, the modification of GCE with CoNiP@rGO results in a substantial increase in peak current (with an equivalent sensitivity of I_{pa}/C of 39 mA M^{-1}), approximately 10.8 times greater than that of GCE. Moreover, the peak potential shifts by about 80 mV towards lower potentials (0.47 V for CoNiP@rGO). These outcomes are attributed to the enhanced sensing properties of CoNiP@rGO, including efficient charge transfer, large surface area, and the synergistic interaction between CoNiP and rGO, contributing to the improved catalytic performance [42].

The electrocatalytic oxidation of BPA at CoNiP@rGO was further characterized by CV at different scan rates (10–100 mV s^{-1}) in a 0.1 M PBS solution containing 250 μM of BPA. The results reveal a linear increase in peak current with the scan rate (Fig. 3c), accompanied by a displacement of the peak potential towards the positive side (Fig. 3d). The linear correlation of I_{pa} indicates that the electro-oxidation of BPA follows an adsorption-controlled process at CoNiP@rGO/GCE. Furthermore, the linear relationship of E_{pa} *vs* ln υ (Fig. 3d) with a significant regression coefficient ($r^2 = 0.9965$) validates the applicability of the Laviron equation, where the irreversible adsorption-controlled electrode processes can be described by **equation (3)** [54]:

$$E_{pa} = E^0 + \frac{RT}{\alpha nF} ln \frac{RTk^0}{\alpha nF} + \frac{RT}{\alpha nF} ln\, \upsilon \tag{3}$$

where E^0 represents the formal redox potential, R denotes the molar gas constant (8.314 J K^{-1} mol^{-1}), T refers to temperature (298 K),

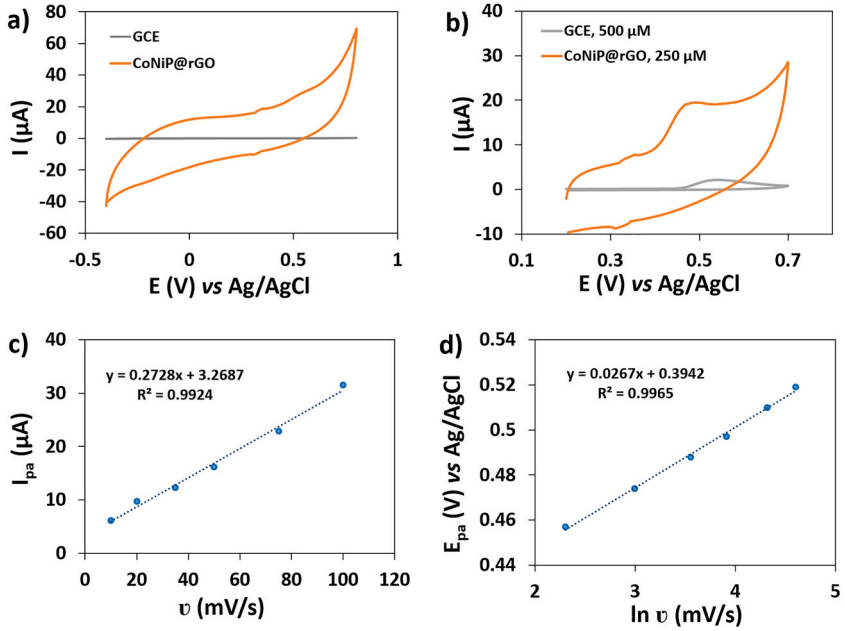

Fig. 3. Cyclic voltammograms recorded at 20 mV s^{-1} (a, b) and cyclic voltammetric data recorded at different scan rates (c, d) of bare GCE and CoNiP@rGO/GCE: (a) from 0.1 M PBS in the absence of BPA; (b) from 0.1 M PBS containing 500 μM of BPA (GCE) or 250 μM of BPA (CoNiP@rGO/GCE); (c) Plot of I_{pa} *vs* υ for CoNiP@rGO/GCE; (d) Plot of the anodic peak potential (E_{pa}) *vs* ln υ.

α represents the electron transfer coefficient (for an irreversible process can be considered as 0.5), F stands for the Faraday's constant (96 480C mol^{-1}), and k^0 is the standard rate constant of the reaction. The calculated number of electron transfer (n) involved in the reaction was estimated to be 1.92, very close to 2, in accordance with the results of previous findings [5,55,56]. In conclusion, the electrochemical oxidation of BPA at CoNiP@rGO/GCE is an irreversible process controlled by adsorption, involving the transfer of two electrons. The observed increase in peak current is assigned to the decrease of charge transfer resistance and the accumulation of BPA at the electrode surface resulting from the adsorption process.

3.3. Electrochemical sensing performance of CoNiP@rGO towards BPA

Given that the electro-oxidation of BPA follows an adsorption-controlled process at the CoNiP@rGO/GCE electrode, the surface concentration of BPA can be enhanced by establishing favourable conditions of potential and time before its detection. As there was no observable variation in I_{pa} for different accumulation potentials, a value of 0 V *vs* Ag/AgCl, *sat.* was chosen for the following investigations of the accumulation time effect. Results obtained for different accumulation times are summarized in Fig. 4, where the peak current from CV was recorded using a 20 μM BPA solution in 0.1 M PBS. The I_{pa} values increased with prolonged accumulation times from 100 to 500 s, but then exhibited a decline when the accumulation time was further extended to 600 s. This decrease can be explained by considering the adsorption of reaction by-products and solution impurities at the electrode surface creating a barrier that inhibits further adsorption of reactants, leading to a decrease in the measured oxidation currents. Based on these findings, an accumulation time of 500 s was deemed optimal for the quantitative determination of BPA.

To assess the electrochemical sensing performance of CoNiP@rGO/GCE for different concentrations of BPA, differential pulse voltammetry was employed after an accumulation time of 500 s at 0 V (Fig. 5a). DPV was chosen for BPA determination due to its higher sensitivity and selectivity, with enhanced signal-to-noise ratio, enabling lower detection limits, compared to CV. Furthermore, the peak-shaped DPV signals offer enhanced effectiveness in complex samples, as they enable more efficient separation of the BPA signal from interference by other co-existing electroactive species.

The peak currents from the DPV voltammograms recorded for different concentrations ranging from 1 nM to 8 μM were plotted against concentrations (Fig. 5b). The correlation coefficient for this set of 10 standard solutions was found to be 0.9992, confirming the suitability of the linear model to describe the calibration curve. Calculated values for the LOD and LOQ were 0.38 nM and 1.26 nM, respectively, applying **equations 1** and **2** to the measurement replicates of the lowest concentration standard. These values fall below the parametric values set for BPA by the European Parliament and the Council (11 nM), indicating that the developed sensor and its operation are not only suitable for detection but also for the quantification of this contaminant in water intended for human consumption. Additionally, the sensitivity of the fabricated sensor is considerably high, with a value of 96.4 A M^{-1} cm^{-2}. Reproducibility and repeatability were also evaluated to characterize the sensor's performance. As illustrated in Fig. 5c, measurements from five independent CoNiP@rGO/GCE electrodes in a 1 μM BPA solution exhibited similar electrochemical signals, with a relative standard deviation (RSD) of only 3.3 %. Similarly, the RSD of seven consecutive measurements using the same electrode in a 1 μM BPA (Fig. 5d) was 3.9 %. These results indicate that the reproducibility and repeatability are quite good, establishing the precision of measurements with this sensor.

The selectivity of the CoNiP@rGO/GCE electrode's response was investigated by evaluating the current response of potential interference organic molecules namely, 4-nitrophenol, 4-aminophenol, and phenol with 10-fold concentrations via DPV, following a 500 s accumulation at 0 V *vs* Ag/AgCl. Fig. 6 presents the current response normalized by the concentration of each species, demonstrating the electrode's capability to selectively detect BPA.

The results suggest that the CoNiP@rGO/GCE sensor exhibits significantly higher sensitivity to BPA compared to other phenolic compounds, indicating that the presence of these compounds would not introduce interference. This conclusion is supported by the substantial difference in the E_p of these potential interfering substances compared to that of BPA, except for phenol whose peak appears

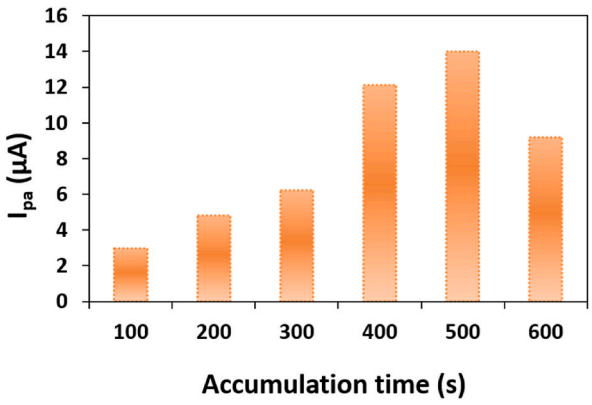

Fig. 4. Accumulation time effect on the anodic peak current of CoNiP@rGO/GCE in 0.1 M PBS containing 20 μM BPA using cyclic voltammetry at a scan rate of 20 mV s^{-1}.

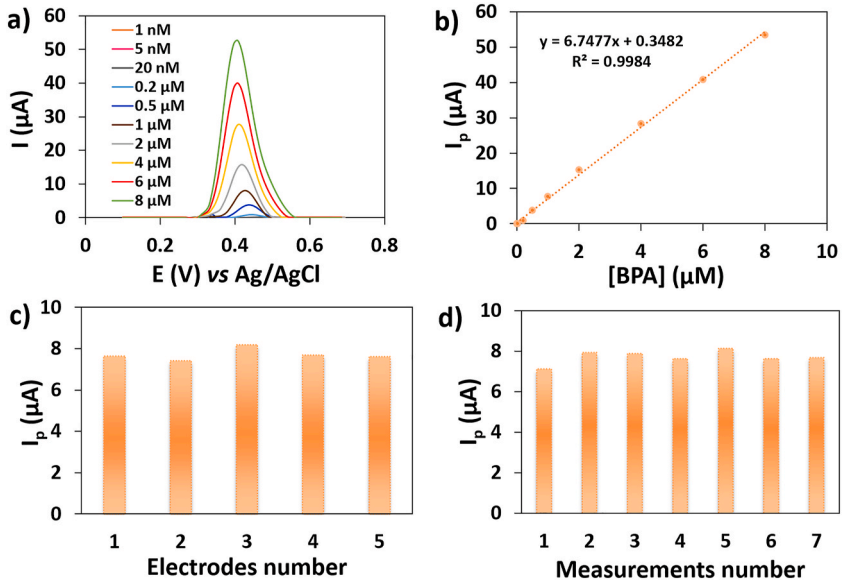

Fig. 5. (a) DPV results of CoNiP@rGO/GCE in 0.1 M PBS comprising distinct concentrations of BPA. (b) Linear calibration curve of the oxidation peak current response *vs* BPA concentrations with an accumulation time of 500 s at 0 V. Anodic peak currents of CoNiP@rGO/GCE in 0.1 M PBS containing 1 µM BPA from (c) five different electrodes and from (d) seven consecutive measurements at a single electrode.

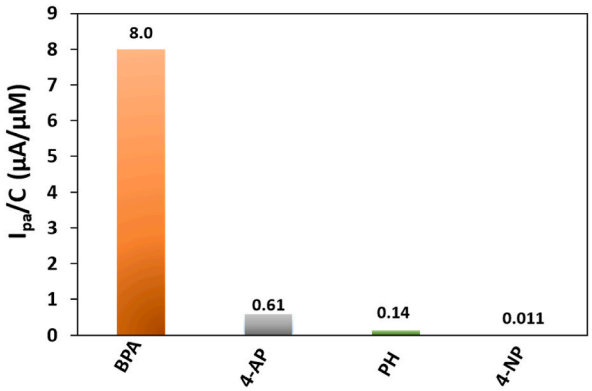

Fig. 6. DPV peak currents of CoNiP@rGO/GCE for different interference organic molecules. The I_{pa}/C values were obtained from a 2 µM solution of BPA and a 20 µM solution of potential interference molecules. The I_p values were determined for E_{pa} of each substance: 4-AP (4-aminophenol, 0.169 V, 12.1 µA); PH (Phenol, 0.487 V, 2.72 µA); 4-NP (4-nitrophenol, 0.239 V, 0.215 µA).

60 mV after the BPA peak.

Assessing the most common performance parameters, sensitivity, linear range, and LOD enables a comparison of the CoNiP@rGO/GCE sensor with other electrochemical sensors for BPA, as summarized in Table 1. Among these sensors, only four (including the CoNiP@rGO/GCE sensor) are suitable for BPA quantification, boasting a LOQ below the parametric value. The CoNiP@rGO/GCE sensor distinguishes itself as one of the top three sensors in each performance parameter, demonstrating a combination of high sensitivity, a broad linear range, and a low LOD.

The performance of the electrochemical sensor was assessed in the determination of BPA in real water samples, specifically bottled and tap water. The samples were spiked at two concentration levels and analysed using the optimized procedure, which involves acquiring DPV voltammogram after an accumulation period of 500 s at 0 V *vs* Ag/AgCl. The recoveries obtained from the spiked tap water and mineral bottled water samples, as well as their RSD are presented in Table 2. The percent recovery values fall within the range of 81–108 %, with RSD levels below 8.4 %. The satisfactory results of the recovery assays affirm the sensor's capability to accurately determine BPA concentrations in both tap and bottled water. Combining these findings with earlier results, it can be concluded that the CoNiP@rGO/GCE sensor is well-suited for the efficient, reliable and accurate detection of BPA in real water samples.

Table 1
Performance comparison of CoNiP@rGO/GCE with other reported electrochemical sensors for BPA detection.

Electrode material	Method	Linear range (μM)	Sensitivity (A M^{-1} cm^{-2})	LOD (nM)	[b)]LOQ (nM)	Ref.
$CoFe_2O_4$/GCE	DPV	0.05–10	0.815	3.6	12	[6]
MAC-Co-SPE	DPV	0.1–350	1.730	10	33.3	[57]
Ni-MOF@CNTs/GCE	DPV	0.001–1	284.6	0.35	*1.17	[58]
Cu_2O-rGO/GCE	Amp	0.1–80	[a)]*3.504 (A M^{-1})*	53	176.7	[41]
NiNP/NCN/CS/GCE	DPV	0.1–2.5	5.42	45	150	[38]
		2.5–15.0	1.85			
$NiFe_2O_4$-rGO/SPE	DPV	0.05–25	4.87	10	33.3	[39]
NiS_2/MoS_2/rGO/GCE	DPV	0.02–200	[a)]*0.2646 (A M^{-1})*	2.1	*7	[55]
FxGnP-Ni-MOF	Amp	0.002–10	0.248	0.184	0.613	[56]
MoS_2–CoS_2/rGO	DPV	0.02–200	[a)]*0.223 (A M^{-1})*	2.5	*8.33	[10]
WO_3-CNT/GCE	DPV	0.03–3.0	11.54	16.3	54.3	[40]
MWCNTs-βCD/SPCE	LSV	0.125–2	101.4	13.7	45.7	[59]
		2–30	30.4			
Ag_2O NCs/Pt	CV	0.08–4.8	95	20	66.7	[60]
CoNiP@rGO/GCE	DPV	0.001–8	6.75	0.38	*1.26	This work
			96.4			

a) The area of the electrode was not mentioned; b) The LOQ was calculated from LOD values using **equation (1)** and **2;** *Sensors that are fitted to the parametric value.

Table 2
BPA determination in real samples using the CoNiP@rGO/GCE (n = 3).

Samples	Spiked (μM)	Detected concentration (μM)	Recovery (%)	RSD (%)
Bottled water	2	2.16	108	6.5
	4	4.15	103	8.4
Tap water	2	1.62	81	6.0
	4	3.97	99	8.0

4. Conclusions

Nanoparticles comprising bimetallic transition metal phosphide, CoNiP, anchored on reduced graphene oxide were synthesized through a solution-based chemical reduction followed by a phosphorization process. This nanocomposite, denoted as CoNiP@rGO, demonstrated remarkable electrochemical sensing capabilities for BPA. The electronic modulation between CoNiP and rGO contributed to the exceptional properties of the CoNiP@rGO, including large surface area, lower charge transfer resistance, and the ability to adsorb BPA. These features collectively led to enhanced electrocatalytic activity for BPA detection when compared to bare GCE. The sensing performance of CoNiP@rGO/GCE was initially assessed using HQ, a model polyphenol, with diffusion-controlled oxidation. CoNiP@rGO/GCE exhibited a wide linear range (0.25−25 μM) for HQ, with boasting a sensitivity of 36.4 A M^{-1} cm^{-2} and an impressive low limit of detection as low as 0.5 μM. Additionally, the sensor demonstrated good reproducibility and repeatability. For the detection of BPA, CoNiP@rGO/GCE exhibited a remarkable low LOD of 0.38 nM and a high sensitivity of 96.4 A M^{-1} cm^{-2}. These values surpass or are comparable to those reported for previously developed sensors, showcasing superior figures of merit. Further validating its practical application, CoNiP@rGO/GCE was successfully employed to detect BPA in real water samples, demonstrating good recovery ranges and low relative standard deviation. This underscores the potential of CoNiP@rGO as an excellent sensing material for detecting phenolic compounds in water, in particularly for the practical application of BPA detection.

Data availability statement

Data associated with the study has not been deposited into a publicly available repository. Data will be made available on request.

CRediT authorship contribution statement

Isilda Amorim: Writing – original draft, Methodology, Investigation, Formal analysis, Data curation, Conceptualization. **Zhipeng Yu:** Investigation, Formal analysis. **Lifeng Liu:** Writing – review & editing, Validation, Supervision, Resources, Funding acquisition, Conceptualization. **Fátima Bento:** Writing – review & editing, Validation, Supervision, Resources, Funding acquisition, Conceptualization.

Declaration of competing interest

The authors declare that they have no known competing financial interests or personal relationships that could have appeared to influence the work reported in this paper.

Acknowledgments

Thanks are due to Fundação para a Ciência e Tecnologia (FCT), Portugal and FEDER (European Fund for Regional Development)-COMPETE-QRENEU for financial support through the research units Chemistry Research Centre of (UID/QUI/00686/2020). I. Amorim is thankful to Fundação para a Ciência e Tecnologia (FCT) for the support of PhD grant No. SFRH/BD/137546/2018 and COVID/BD/153233/2023, co-financed by the Fundo Social Europeu (FSE) through the Programa Operacional Regional Norte (Norte 2020) under Portugal 2020.

References

[1] H. Meskher, F. Achi, Electrochemical Sensing Systems for the Analysis of Catechol and Hydroquinone in the Aquatic Environments: A Critical Review, Crit Rev Anal Chem, 2022.
[2] D. Manoj, S. Rajendran, T.K.A. Hoang, M. Soto-Moscoso, The role of MOF based nanocomposites in the detection of phenolic compounds for environmental remediation- A review, Chemosphere 300 (2022) 134516.
[3] W.W. Anku, M.A. Mamo, P.P. Govender, Phenolic compounds in water: sources, reactivity, toxicity and treatment methods, in: M. Soto-Hernandez, M. Palma-Tenango, M.d.R. Garcia-Mateos (Eds.), Phenolic Compounds - Natural Sources, Importance and Applications, InTech, Rijeka, 2017, p. 17.
[4] T.S.S.K. Naik, S. Singh, N. Pavithra, R. Varshney, B. Uppara, J. Singh, N.A. Khan, L. Singh, M.Z. Arshad, P.C. Ramamurthy, Advanced experimental techniques for the sensitive detection of a toxic bisphenol A using UiO-66-NDC/GO-based electrochemical sensor, Chemosphere 311 (2023) 137104.
[5] M. Annalakshmi, T.S.T. Balamurugan, S. Kumaravel, S.M. Chen, J.L. He, Facile hydrothermal synthesis of manganese sulfide nanoelectrocatalyst for high sensitive detection of Bisphenol A in food and eco-samples, Food Chem. 393 (2022) 133316.
[6] Q. Liu, X.Z. Kang, L.Z. Xing, Z.X. Ye, Y.C. Yang, A facile synthesis of nanostructured CoFe2O4 for the electrochemical sensing of bisphenol A, RSC Adv. 10 (2020) 6156–6162.
[7] G. Kesavan, N. Nataraj, S.M. Chen, L.H. Lin, Hydrothermal synthesis of NiFe2O4 nanoparticles as an efficient electrocatalyst for the electrochemical detection of bisphenol A, New J. Chem. 44 (2020) 7698–7707.
[8] J. Ahmed, M.M. Rahman, I.A. Siddiquey, A.M. Asiri, M.A. Hasnat, Efficient Bisphenol-A detection based on the ternary metal oxide (TMO) composite by electrochemical approaches, Electrochim. Acta 246 (2017) 597–605.
[9] T.D. Vu, P.K. Duy, H.T. Bui, S.H. Han, H. Chung, Reduced graphene oxide-Nickel sulfide (NiS) composited on mechanical pencil lead as a versatile and cost-effective sensor for electrochemical measurements of bisphenol A and mercury (II), Sensor Actuat B-Chem 281 (2019) 320–325.
[10] J.J. Yuan, B.J. Huang, Y.C. Lu, L. Jiang, G.Y. He, H.Q. Chen, Ultrasensitive electrochemical detection of bisphenol A using composites of MoS2 nanoflowers, CoS2 nano-polyhedrons and reduced graphene oxide, Environ. Chem. Lett. 20 (2022) 2751–2756.
[11] Y.H. Duan, S. Li, S. Lei, J.T. Qiao, L.N. Zou, B.X. Ye, Highly sensitive determination of bisphenol A based on MoCuSe nanoparticles decorated reduced graphene oxide modified electrode, J. Electroanal. Chem. 827 (2018) 137–144.
[12] R.G. Shi, J. Liang, Z.S. Zhao, Y. Liu, A.F. Liu, In situ determination of bisphenol A in beverage using a molybdenum selenide/reduced graphene oxide nanoparticle composite modified glassy carbon electrode, Sensors-Basel 18 (2018) 1660.
[13] X.D. Xin, S.H. Sun, H. Li, M.Q. Wang, R.B. Jia, Electrochemical bisphenol A sensor based on core-shell multiwalled carbon nanotubes/graphene oxide nanoribbons, Sensor Actuat B-Chem 209 (2015) 275–280.
[14] T.C. Canevari, M.V. Rossi, A.D.P. Alexiou, Development of an electrochemical sensor of endocrine disruptor bisphenol A by reduced graphene oxide for incorporation of spherical carbon nanoparticles, J. Electroanal. Chem. 832 (2019) 24–30.
[15] X.W. Dong, X.L. Qi, N. Liu, Y.S. Yang, Y.X. Piao, Direct electrochemical detection of bisphenol A using a highly conductive graphite nanoparticle film electrode, Sensors-Basel 17 (2017) 836.
[16] W.H. Zheng, Z.L. Xiong, H.F. Li, S.M. Yu, G.G. Li, L.T. Niu, W.L. Liu, Electrodeposited Pt@Molecularly imprinted polymer core-shell nanostructure: enhanced sensing platform for sensitive and selective detection of bisphenol A, Sensor Actuat B-Chem 272 (2018) 655–661.
[17] K. Shim, J. Kim, M. Shahabuddin, Y. Yamauchi, M.S.A. Hossaina, J.H. Kim, Efficient wide range electrochemical bisphenol-A sensor by self-supported dendritic platinum nanoparticles on screen-printed carbon electrode, Sensor Actuat B-Chem 255 (2018) 2800–2808.
[18] L. Wu, H. Yan, J. Wang, G.J. Liu, W.H. Xie, Tyrosinase incorporated with Au-Pt@SiO2 nanospheres for electrochemical detection of bisphenol A, J. Electrochem. Soc. 166 (2019) B562–B568.
[19] A. Agarwal, B.R. Sankapal, Metal phosphides: topical advances in the design of supercapacitors, J. Mater. Chem. A 9 (2021) 20241–20276.
[20] L.S. Xie, A.M. Asiri, X.P. Sun, Monolithically integrated copper phosphide nanowire: an efficient electrocatalyst for sensitive and selective nonenzymatic glucose detection, Sensor Actuat B-Chem 244 (2017) 11–16.
[21] X.L. Xiong, C. You, X.Q. Cao, L.F. Pang, R.M. Kong, X.P. Sun, Ni2P nanosheets array as a novel electrochemical catalyst electrode for non-enzymatic H2O2 sensing, Electrochim. Acta 253 (2017) 517–521.
[22] H.F. Zhou, M.L. Cui, Y. Zhao, C. Wang, Q.J. Song, Preparation of nitrogen and FeP doped carbon nanotubes for selective and simultaneous electrochemical detection of dihydroxybenzoic acid isomers, Electrochim. Acta 242 (2017) 107–116.
[23] X.B. Liu, F.Y. He, L.W. Bai, X.W. Cao, C. Liu, W.B. Lu, A two-dimensional G-CoP/N,P-co-doped carbon nanowire electrode for the simultaneous determination of hydroquinone and catechol in domestic wastewater, Anal. Chim. Acta 1210 (2022) 339871.
[24] K.D. Wang, C. Wu, F. Wang, G.Q. Jiang, MOF-derived CoPx nanoparticles embedded in nitrogen-doped porous carbon polyhedrons for nanomolar sensing of p-nitrophenol, ACS Appl. Nano Mater. 1 (2018) 5843–5853.
[25] L.L. Xiao, R.Y. Xu, F. Wang, Facile synthesis of CoxP decorated porous carbon microspheres for ultrasensitive detection of 4-nitrophenol, Talanta 179 (2018) 448–455.
[26] O.C. Compton, S.T. Nguyen, Graphene oxide, highly reduced graphene oxide, and graphene: versatile building blocks for carbon-based materials, Small 6 (2010) 711–723.
[27] R. Tarcan, O. Todor-Boer, I. Petrovai, C. Leordean, S. Astilean, I. Botiz, Reduced graphene oxide today, J. Mater. Chem. C 8 (2020) 1198–1224.
[28] B. Li, G.H. Pan, N.D. Avent, R.B. Lowry, T.E. Madgett, P.L. Waines, Graphene electrode modified with electrochemically reduced graphene oxide for label-free DNA detection, Biosens. Bioelectron. 72 (2015) 313–319.
[29] Q. Cao, B. Kumru, M. Antonietti, B.V.K.J. Schmidt, Graphitic carbon nitride and polymers: a mutual combination for advanced properties, Mater. Horiz. 7 (2020) 762–786.
[30] R. Gautam, N. Marriwala, R. Devi, A review: study of Mxene and graphene together, Measurement: Sensors 25 (2023) 100592.
[31] J.L. Zheng, X. Pan, X.M. Huang, D.B. Xiong, Y. Shang, X.X. Li, N. Wang, W.M. Lau, H.Y. Yang, Integrated NiCo2-LDHs@MXene/rGO aerogel: componential and structural engineering towards enhanced performance stability of hybrid supercapacitor, Chem Eng J 396 (2020) 125197.
[32] E.M. Kirchner, T. Hirsch, Recent developments in carbon-based two-dimensional materials: synthesis and modification aspects for electrochemical sensors, Microchim. Acta 187 (2020) 441.
[33] A.Y.S. Tan, N.W. Lo, F.L. Cheng, M. Zhang, M.T.T. Tan, S. Manickam, K. Muthoosamy, 2D carbon materials based photoelectrochemical biosensors for detection of cancer antigens, Biosens. Bioelectron. 219 (2023) 14811.
[34] C. Jing, X.Y. Song, K.L. Li, Y.M. Zhang, X.Y. Liu, B.Q. Dong, F. Dong, S.L. Zhao, H.C. Yao, Y.X. Zhang, Optimizing the rate capability of nickel cobalt phosphide nanowires on graphene oxide by the outer/inter-component synergistic effects, J. Mater. Chem. A 8 (2020) 1697–1708.

[35] X.X. Zhao, Y.P. Fan, H.Y. Wang, C.Y. Gao, Z.Y. Liu, B.J. Li, Z.K. Peng, J.H. Yang, B.Z. Liu, Cobalt phosphide-embedded reduced graphene oxide as a bifunctional catalyst for overall water splitting, ACS Omega 5 (2020) 6516–6522.
[36] B. Koo, S. Byun, S.W. Nam, S.Y. Moon, S. Kim, J.Y. Park, B.T. Ahn, B. Shin, Reduced graphene oxide as a catalyst binder: greatly enhanced photoelectrochemical stability of Cu(in,Ga)Se-2 photocathode for solar water splitting, Adv. Funct. Mater. 28 (2018) 1705136.
[37] L.J. Liu, R.F. Chen, W.K. Liu, J.M. Wu, D. Gao, Catalytic reduction of 4-nitrophenol over Ni-Pd nanodimers supported on nitrogen-doped reduced graphene oxide, J. Hazard Mater. 320 (2016) 96–104.
[38] Y. Wang, C. Yin, Q.F. Zhuang, An electrochemical sensor modified with nickel nanoparticle/nitrogen-doped carbon nanosheet nanocomposite for bisphenol A detection, J. Alloys Compd. 827 (2020) 154335.
[39] S.Z. Bas, N. Yuncu, K. Atacan, M. Ozmen, A comparison study of MFe2O4 (M: Ni, Cu, Zn)-reduced graphene oxide nanocomposite for electrochemical detection of bisphenol A, Electrochim. Acta 386 (2021) 138519.
[40] Y. Zhou, X.Y. She, Q. Wu, J.R. Xiao, T.Y. Peng, Monoclinic WO3 nanosheets-carbon nanotubes nanocomposite based electrochemical sensor for sensitive detection of bisphenol A, J. Electroanal. Chem. 915 (2022) 116355.
[41] R.G. Shi, J. Liang, Z.S. Zhao, A.F. Liu, Y. Tian, An electrochemical bisphenol A sensor based on one step electrochemical reduction of cuprous oxide wrapped graphene oxide nanoparticles modified electrode, Talanta 169 (2017) 37–43.
[42] I. Amorim, Z. Yu, F. Bento, L. Liu, Towards an improved electrocatalytic material for detection of polyphenols based on transition metal phosphides anchored on reduced graphene oxide, J. Electrochem. Soc. 170 (2023) 027506.
[43] J.Y. Xu, J.J. Li, D.H. Xiong, B.S. Zhang, Y.F. Liu, K.H. Wu, I. Amorim, W. Li, L.F. Liu, Trends in activity for the oxygen evolution reaction on transition metal (M = Fe, Co, Ni) phosphide precatalysts, Chem. Sci. 9 (2018) 3470–3476.
[44] S.J. Konopka, B. McDuffie, Diffusion coefficients of ferri- and ferrocyanide ions in aqueous media, using twin-electrode thin-layer electrochemistry, Anal. Chem. 42 (1970) 1741–1746.
[45] L.M. Fan, X.Y. Li, X.W. Kan, Disposable graphite paper based sensor for sensitive simultaneous determination of hydroquinone and catechol, Electrochim. Acta 213 (2016) 504–511.
[46] L.A. Alshahrani, L.Y. Liu, P. Sathishkumar, J.M. Nan, F.L. Gu, Copper oxide and carbon nano-fragments modified glassy carbon electrode as selective electrochemical sensor for simultaneous determination of catechol and hydroquinone in real-life water samples, J. Electroanal. Chem. 815 (2018) 68–75.
[47] T.T. Chen, J.Q. Xu, M. Arsalan, Q.L. Sheng, J.B. Zheng, W. Cao, T.L. Yue, Controlled synthesis of Au@Pd core-shell nanocomposites and their application for electrochemical sensing of hydroquinone, Talanta 198 (2019) 78–85.
[48] Y.H. Huang, J.H. Chen, X. Sun, Z.B. Su, H.T. Xing, S.R. Hu, W. Weng, H.X. Guo, W.B. Wu, Y.S. He, One-pot hydrothermal synthesis carbon nanocages-reduced graphene oxide composites for simultaneous electrochemical detection of catechol and hydroquinone, Sensor Actuat B-Chem 212 (2015) 165–173.
[49] M.F. Cao, Y.J. Zou, Y.Y. Zhang, T. Zeng, Q.J. Wan, G.S. Lai, N.J. Yang, Robust and selective electrochemical sensing of hazardous photographic developing agents using a MOF-derived 3D porous flower-like Co3O4@C/graphene nanoplate composite, Electrochim. Acta 409 (2022) 139967.
[50] M. Nazari, S. Kashanian, P. Moradipour, N. Maleki, A novel fabrication of sensor using ZnO-Al2O3 ceramic nanofibers to simultaneously detect catechol and hydroquinone, J. Electroanal. Chem. 812 (2018) 122–131.
[51] R.Y. Xu, L.L. Xiao, L. Luo, Q.H. Yuan, D.F. Qin, G.Z. Hu, W. Gan, Nitrogen, sulfur dual-doped mesoporous carbon modified glassy carbon electrode for simultaneous determination of hydroquinone and catechol, J. Electrochem. Soc. 163 (2016) B617–B623.
[52] C.B. Liu, K. Wang, S.L. Luo, Y.H. Tang, L.Y. Chen, Direct electrodeposition of graphene enabling the one-step synthesis of graphene-metal nanocomposite films, Small 7 (2011) 1203–1206.
[53] L.Y. Chen, Y.H. Tang, K. Wang, C.B. Liu, S.L. Luo, Direct electrodeposition of reduced graphene oxide on glassy carbon electrode and its electrochemical application, Electrochem. Commun. 13 (2011) 133–137.
[54] E. Laviron, General expression of the linear potential sweep voltammogram in the case of diffusionless electrochemical systems, J. Electroanal. Chem. 101 (1979) 19–28.
[55] J.J. Yuan, L. Jiang, J.F. Che, G.Y. He, H.Q. Chen, Composites of NiS2 microblocks, MoS2 nanosheets, and reduced graphene oxide for energy storage and electrochemical detection of bisphenol A, ACS Appl. Nano Mater. 4 (2021) 6093–6102.
[56] P. Arul, S.T. Huang, N.S.K. Gowthaman, G. Mani, N. Jeromiyas, S. Shankar, S.A. John, Electrocatalyst based on Ni-MOF intercalated with amino acid-functionalized graphene nanoplatelets for the determination of endocrine disruptor bisphenol A, Anal. Chim. Acta 1150 (2021) 338228.
[57] F. Emambakhsh, H. Asadollahzadeh, N. Rastakhiz, S.Z. Mohammadi, Highly sensitive determination of Bisphenol A in water and milk samples by using magnetic activated carbon - cobalt nanocomposite-screen printed electrode, Microchem. J. 179 (2022) 107466.
[58] C.X. Xu, L.B. Liu, C. Wu, K.B. Wu, Unique 3D heterostructures assembled by quasi-2D Ni-MOF and CNTs for ultrasensitive electrochemical sensing of bisphenol A, Sensor Actuat B-Chem 310 (2020) 127885.
[59] M.Y. Ali, A. Ul Alam, M.M.R. Howlader, Fabrication of highly sensitive Bisphenol A electrochemical sensor amplified with chemically modified multiwall carbon nanotubes and beta-cyclodextrin, Sensor Actuat B-Chem 320 (2020) 128319.
[60] U. Chakraborty, G. Bhanjana, G. Kaur, A. Kaushik, G.R. Chaudhary, Electro-active silver oxide nanocubes for label free direct sensing of bisphenol A to assure water quality, Mater. Today Chem. 16 (2020) 100267.